Seismic fragility curves of bridge piers accounting for ground motions in Korea

Duy-Duan Nguyen[1,2*] and Tae-Hyung Lee[1]

[1] Department of Civil Engineering, Konkuk University, Seoul 05029, Korea
[2] Department of Civil Engineering, Vinh University, Vinh 461010, Vietnam
[*] Corresponding author, email: duyduan@konkuk.ac.kr

Abstract. Korea is located in a slight-to-moderate seismic zone. Nevertheless, several studies pointed that the peak earthquake magnitude in the region can be reached to approximately 6.5. Accordingly, a seismic vulnerability evaluation of the existing structures accounting for ground motions in Korea is momentous. The purpose of this paper is to develop seismic fragility curves for bridge piers of a steel box girder bridge equipped with and without base isolators based on a set of ground motions recorded in Korea. A finite element simulation platform, OpenSees, is utilized to perform nonlinear time history analyses of the bridges. A series of damage states is defined based on a damage index which is expressed in terms of the column displacement ductility ratio. The fragility curves based on Korean motions were thereafter compared with the fragility curves generated using worldwide earthquakes to assess the effect of the two ground motion groups on the seismic fragility curves of the bridge piers. The results reveal that both non- and base-isolated bridge piers are less vulnerable during the Korean ground motions than that under worldwide earthquakes.

1. Introduction

Fragility curve is a useful tool for seismic vulnerability assessment of infrastructures. In recent years, many researchers developed fragility curves for structures not only based on empirical methods but also analytical procedures. Developing fragility functions from empirical observations sometimes encounter challenges due to lack of sufficient damage data caused by past earthquakes. In an alternative way, fragility curves can be constructed by applying some analytical procedures such as elastic spectral analysis, nonlinear static analysis, and nonlinear time-history analysis methods [1-2]. Among these analytical methods, nonlinear time history analysis is the most widely used and the most reliable method for deriving fragility curves of structures [2-3]. Some authors developed fragility curves for bridge structures located in various regions applying the nonlinear time-history analysis such as Karim and Yamazaki [4] in Japan, Moschonas et al [5] in Greek, Choi et al [6] in the Central and South Eastern United States, Kibboua et al [7] in Algeria, Tavares et al [8] in Canada, Lee et al [9], Lee and Nguyen [10] in Korea, and Abbasi et al [11] in California. Moreover, the effect of base isolator devices on seismic fragility curves of bridge structures were also considered in elsewhere [12-14].

The previous studies developed fragility curves of different bridge types mostly using of ground motions from worldwide earthquakes. Recently, earthquakes have been occurred in South Korea with a higher level of intensity, such as the 2016 Gyeongju earthquake and the 2017 Pohang earthquake. This study focuses on deriving analytical fragility curves for RC piers of a typical continuous steel box girder bridge in South Korea considering ground motions in the region. The finite element framework, OpenSees [15],

is utilized to perform nonlinear time-history analyses. A damage index is proposed in terms of the displacement ductility ratio [16]. Four damage states, namely slight, moderate, extensive, and collapse are defined based on the proposed damage indices. From the observation of damage levels, fragility curves for the bridge piers are obtained using the maximum likelihood estimation. The fragility curves are then compared with the curves obtained using a group of worldwide ground motions from history earthquake events.

2. Description of the studied bridge

The selected case study bridge is a seven-span continuous steel box girder bridge and supported by six circular RC single column piers. The length of the first and the last three spans is 50m, the length of the second, third and fourth spans is 52.8m, 62.0m, and 54.5m, respectively as shown in Figure 1. The columns height is varied from 10.4m for pier P1, 8.75m for pier P2, 6.8m for pier P6 and 6.5m for both pier P3, pier P4 and pier P5. The cross-sectional diameter of all pier-columns is 1.6m. The cross-sectional dimensions of the bridge girder and the column are depicted in Figure 2 and Figure 3, respectively.

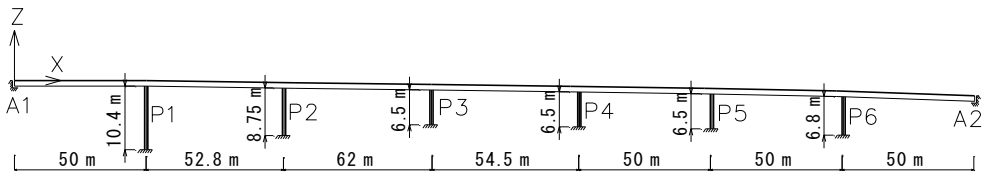

Figure 1. The view of the investigated bridge

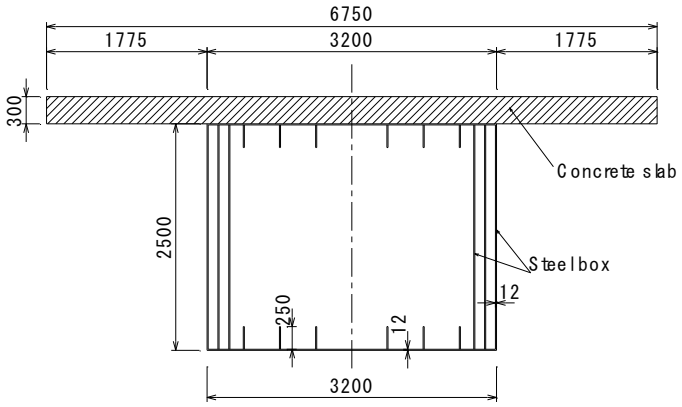

Figure 2. Cross section of the girder

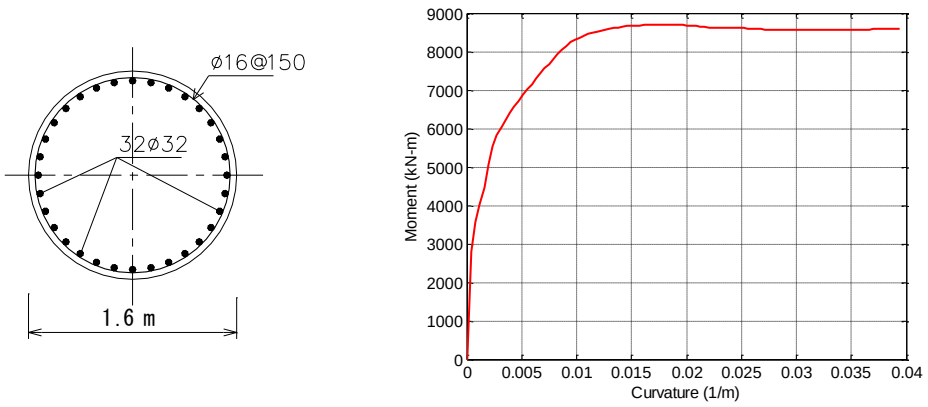

Figure 3. Cross section and moment-curvature relationship of the bridge piers

3. Seismic fragility analysis procedure

To develop the fragility curves for the bridges, nonlinear time history analyses are performed. The procedure for generating fragility curves of the structure can be implemented by basic steps as follows.

1) Set up the bridge models that take into account nonlinear materials as well as the inelastic features of the bridge columns.
2) Apply sets of ground motions with a wide range of peak ground acceleration (PGA) to the bridge models. In this study, two groups of ground motions are considered for nonlinear time history analyses. The first group consists of 20 worldwide ground accelerations from the historic earthquake events and the second one comprises 07 natural and man-made ground accelerations recorded in Korea. For each ground motion, PGA is scaled from 0.1g to 2.0g with intervals of 0.1g in order to consider a wide range of the seismic intensity measure. Consequently, the maximum displacement ductility of the pier columns is obtained.
3) Define the limit states of each component based on the damage index which expressed in terms of ductility ratio of columns.
4) Calculate the sample rate of reaching and exceeding the limit state at each PGA level.
5) Develop fragility curves of bridge piers based on fitting fragility functions to the observed data using the maximum likelihood estimate formulation [3].

A fragility function expresses the probability that the demand on the structure reaches or exceeds the structural capacity at a specific damage state. For this study, the fragility function is assumed as a log-normal cumulative distribution function expressed by

$$P[LS|IM = X] = \Phi\left(\frac{\ln X - \mu}{\beta}\right) \quad (1)$$

where $P[LS \mid IM]$ is the probability of a limit state (LS) at a given ground motion intensity measure (IM); X is the value of ground motion in terms of PGA; μ and β are the median and standard deviation of lnX, respectively; $\Phi(\text{-})$ is standard normal cumulative distribution function.

4. Numerical modelling

4.1. Material model

In OpenSees, there are some proposed models for concrete and steel materials. For this study, the *concrete02* model [17] is applied for confined and unconfined concrete, while the *steel02* model [18] is used for modeling of reinforcing bars in the bridge piers. These two models have taken into account the nonlinearity of materials. The moment-curvature relationship of all column sections is illustrated in Figure 3. Properties of the concrete and the steel are described in Table 1 and Table 2, respectively. In Table 1, f_{pc} is the concrete compressive strength at 28 days, ε_{co} is the concrete strain at maximum strength, f_{pcu} is the concrete crushing strength, ε_u is the concrete strain at crushing strength, ft is the concrete tensile strength, and E_{ts} is the tension softening stiffness. In Table 2, F_y is the yield strength, E_s is the initial elastic stiffness, b is the strain-hardening ratio, R_0 is a constant between 10 and 20, C_{R1} and C_{R2} are coefficients. Figure 4 shows the stress-strain relationship of the concrete and steel material models.

Table 1. Concrete material properties

	f_{pc} (Mpa)	ε_{co}	f_{pcu} (MPa)	ε_u	f_t (MPa)	E_{ts} (GPa)
Confined concrete	40.8	0.004	34.2	0.02	4.0	0.55
Unconfined concrete	27.2	0.002	6.8	0.002	4.0	0.55

Table 2. Steel material properties

	F_y (Mpa)	E_s (GPa)	b	R_0	C_{R1}	C_{R2}
Steel	408	197	0.01	18	0.925	0.15

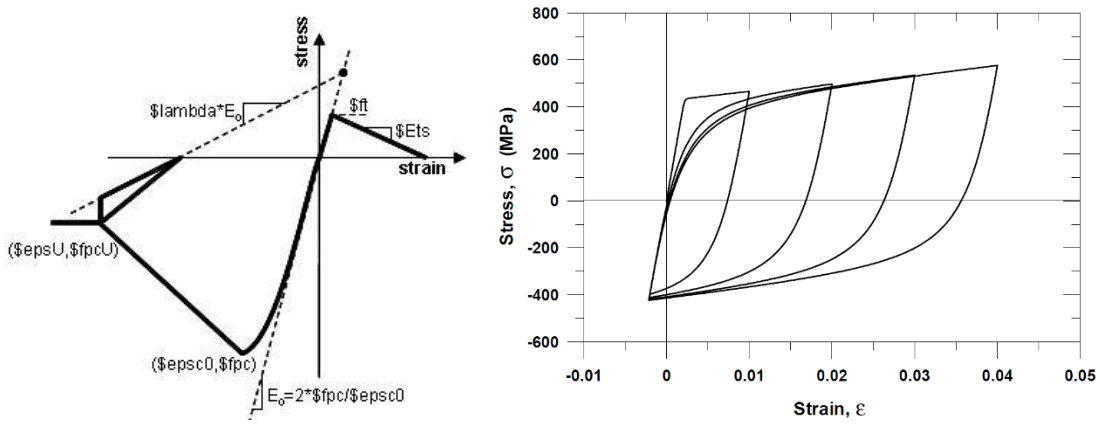

Figure 4. *Concrete02* (left) and *Steel02* (right) models

4.2. Elements modelling

During a strong earthquake, the bridge piers may suffer from experiencing inelastic behavior. For modeling the nonlinear behavior along the element length, the *nonlinearBeamColumn* element with the fiber section modeling scheme is used. The *concrete02* and *steel02* constitutive models are represented for concrete and steel fibers, respectively.

Additionally, the girder is assumed to remain elastic during seismic excitations. Hence, the *elasticBeamColumn* element is adopted to model the bridge girder components. Some characterized quantities of the girder section such as cross-sectional area, torsional moment of inertia of cross section, and second moments of area are calculated from the section in Figure 2. Moreover, the element mass per unit length of the superstructure is also imposed to implement the dynamic analysis procedure of the bridge.

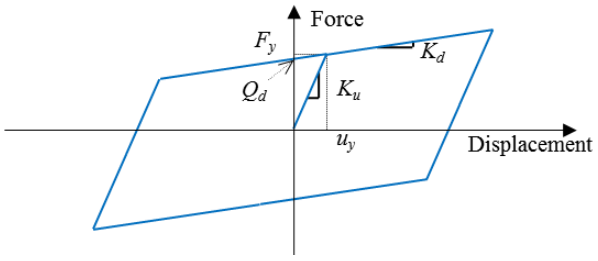

Figure 5. Force-deformation relationship of LRB

For the isolated bridge, one of the most important components of the structure is the connections between substructures and superstructure. On the pier-caps and abutments, the lead rubber bearings (LRBs) are installed to accommodate deformations of the superstructure during earthquake events. The behavior of an LRB under shear forces is assumed to be a bilinear model that is characterized by typical features: initial stiffness (K_u), post-yield stiffness (K_d) and yield strength (F_y) or characteristic strength (Q_d). Figure 5 shows the sketch of the *elastomericBearing* element, which was distinctly designed to apply for modeling a base isolator in OpenSees. Figure 6 shows the modeling of structural components of the base-isolated bridges.

For the non-isolated bridge, the continuous superstructure is rigidly connected to the columns. In OpenSees, this connection is modeled by rigid-link elements. It should be noted that the effect of abutments, as well as soil-structure interaction on performances of the bridge, is neglected in this research. Therefore, the piers are modeled to be fixed on the ground, while the abutment-superstructure connections are modeled as pinned restraints.

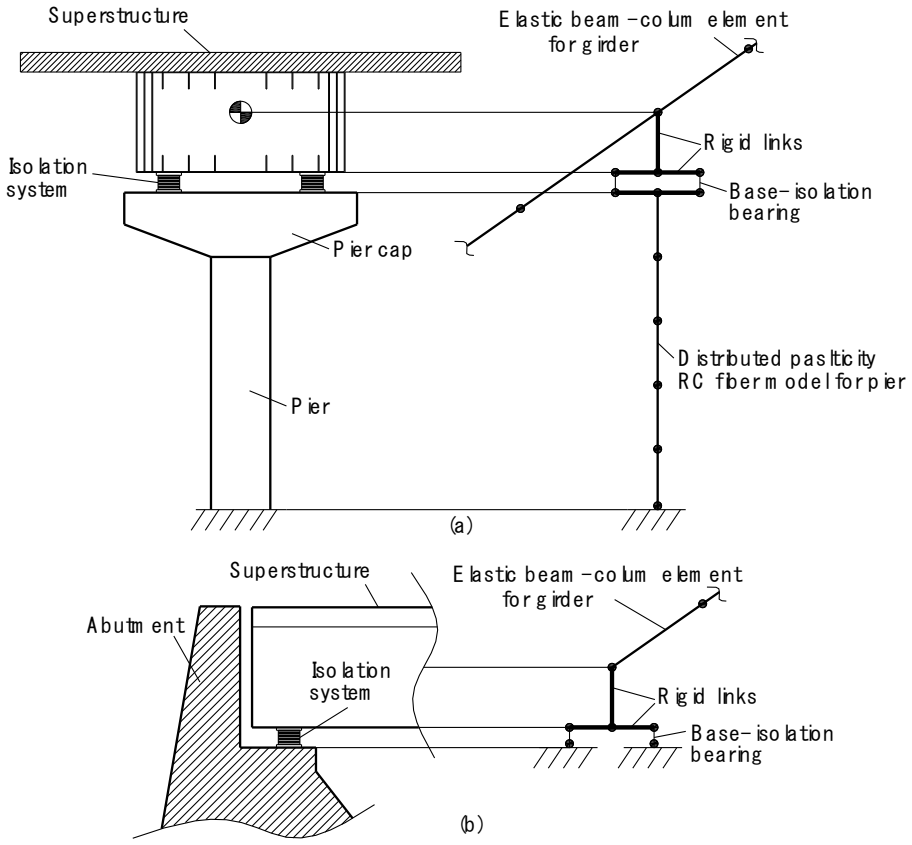

Figure 6. Modeling scheme of the isolated bridge in OpenSees (a) pier-girder and (b) abutment-girder connection

4.3. Vibration modes

Figure 7 shows the first three vibration mode shapes and corresponding natural periods of the studied bridges with and without based isolators. Due to large deformation capacity of LRBs, the inertial force in the girder is reduced and all vibration periods are approximately increased by 1.5 times compared with those of the non-isolated bridge. Table 3 shows the comparison of eigenvalue analysis between two FEM software, OpenSees and SAP2000 [19]. We can observe that the results are highly comparable.

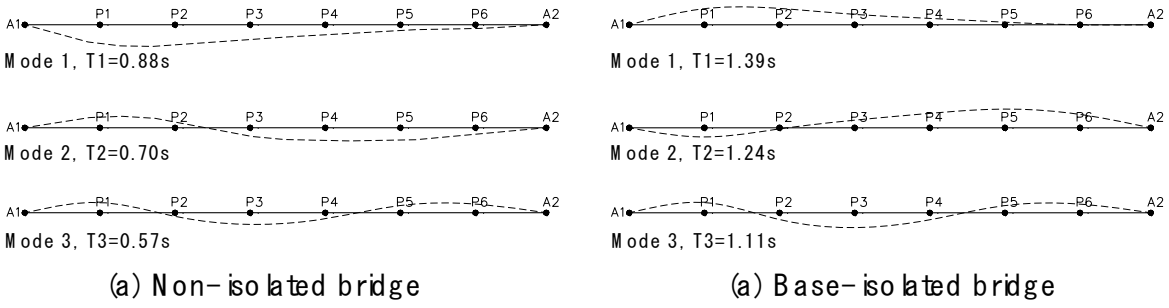

Figure 7. Three natural vibration modes of the bridge models

Table 3. Comparison of natural periods (sec) of the bridge between OpenSees and SAP2000

Mode	OpenSees		SAP2000	
	Non-isolated	Base-isolated	Non-isolated	Base-isolated
Mode 1	0.88	1.39	0.87	1.41
Mode 2	0.70	1.24	0.68	1.25
Mode 3	0.57	1.11	0.54	1.14

5. Ground motions

Twenty worldwide ground accelerations from historic earthquake events and seven natural and man-made ground accelerations in Korea are selected for analyses. The variation of the ground motion profiles has taken into account as a source of uncertainty for the seismic fragility analysis procedure. The magnitude and PGA of the suite of ground motions in Korea are described in Table 4. Figures 8 and 9 show the acceleration and displacement response spectra of the selected ground motions, in which the red bold curve indicates their average response spectrum. It can be seen that the acceleration response spectra in Korean ground motions are very small with periods T > 1.0 sec. In addition, the displacement response spectra in Korean motions are also much smaller than that of worldwide motions.

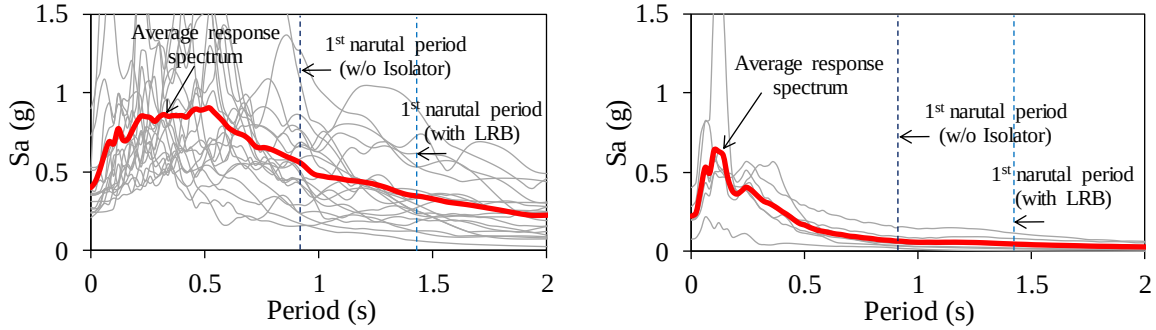

Figure 8. Acceleration response spectra of Worldwide (*left*) and Korean (*right*) ground motions

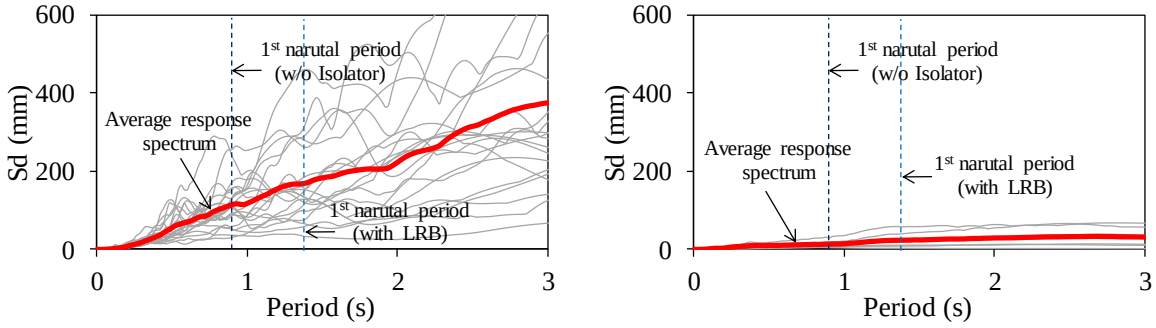

Figure 9. Displacement response spectra of Worldwide (*left*) and Korean (*right*) ground motions

Table 4. List of selected ground motion records in Korea

	Earthquake	Time	Station	Mag. (M)	PGA (g)
1	Gyeongju	2016/09/12	DKJ	5.8	0.078
2	Gyeongju	2016/09/12	MKL	5.8	0.284
3	Gyeongju	2016/09/12	USN	5.8	0.404
4	KESB	-	Artificial 1	-	0.200
5	KESC	-	Artificial 2	-	0.200
6	KESD	-	Artificial 3	-	0.200
7	KESE	-	Artificial 4	-	0.200

6. Seismic response of bridges

Nonlinear time history analyses are carried out for each ground motion in different scaled levels of PGA. The displacement at the top of bridge piers is monitored during seismic excitations. Figure 10 shows the lateral displacement time-history response of piers subjected to the 2016 Gyeongju earthquake for an illustration. Due to the presence of LRBs, the pier displacement at the top is significantly decreased compared with those of the non-isolated bridge piers. It should note that we do compare results of all cases of the bridge equipped with LRBs and non-isolated bridge models accounting for all selected ground motions.

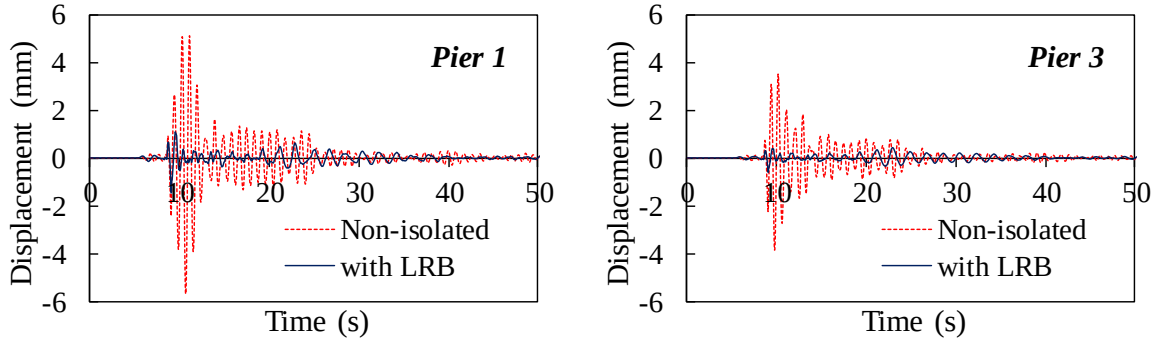

Figure 10. Displacement response of the bridge piers P1 & P3 with and without LRBs during the Gyeongju earthquake (DKJ station, PGA = 0.078g)

7. Damage states and fragility analysis results

Because of the extremely important role of piers, the vulnerability of a pier will affect the load bearing capacity of the entire structure. We only focused on the damage states definition and fragility analysis procedure for the bridge columns, which is the most crucial member of the bridge structure.

For this study, we have adopted the definition of damage states based on column curvature ductility ratio (μ_ϕ) and displacement ductility ratio (μ_Δ) proposed in FHWA [16] for constructing fragility curves of bridge columns. The curvature ductility ratio is expressed as following equation.

$$\mu_\phi = 1 + \frac{\mu_\Delta - 1}{3\frac{l_p}{L}\left(1 - 0.5\frac{l_p}{L}\right)} \tag{2}$$

Due to practice reasons, the damage states related to displacements are more facilitated than use of the curvature ductility. Equation (2) can be rewritten in terms of displacement ductility ratio as

$$\mu_\Delta = 1 + 3\frac{l_p}{L}\left(1 - 0.5\frac{l_p}{L}\right)\left(\mu_\phi - 1\right) \tag{3}$$

where L is the length of the column, l_p is the length of the plastic hinge given by the equation (4) hereafter, d_b is the diameter of the column longitudinal reinforcing bar. It should be noted that curvature ductility ratio (μ_ϕ) can be also defined as the ratio of the developing curvature in the piers due to bending moment to the curvature at the first yielding state of the reinforcement.

$$l_p = 0.08L + 9d_b \tag{4}$$

Accordingly, four damage states (DS), namely, slight, moderate, extensive, and collapse are defined in terms of the column displacement ductility ratio. Table 5 shows damage states of all bridge piers and the corresponding the damage indices. It should be noted that the piers P3, P4 and P5 are all the same height, thus, they are in the same value of the defined damage levels.

Figs 11 and 12 show fragility curves of the bridge piers P1 and P3 equipped with and without LRBs using Korean ground motions. It should be noted that piers P1 and P3 are the high and short piers in the

bridge model, respectively. The result reveals that the bridge equipped with LRBs is less vulnerable than the case of without base isolators. Due to the energy dissipation capacity of the lead plug and the shear deformation capacity of the rubber layers in LRBs, lateral displacement at the top of the bridge piers is significantly reduced under seismic excitations. On the other hand, the short pier (i.e. P3) is more vulnerable than the high pier (i.e. P1) at a specific level of PGA.

Table 5. Proposed damage states of the studied bridges

Component	Demand Parameter	Threshold value			
		Slight (DS1)	Moderate (DS2)	Extensive (DS3)	Collapse (DS4)
Pier P1	Displacement ductility ratio	1.0	1.2	1.9	4.7
Pier P2		1.0	1.3	2.0	4.8
Pier P3, P4, P5		1.0	1.3	2.0	5.2
Pier P6		1.0	1.3	2.0	5.1

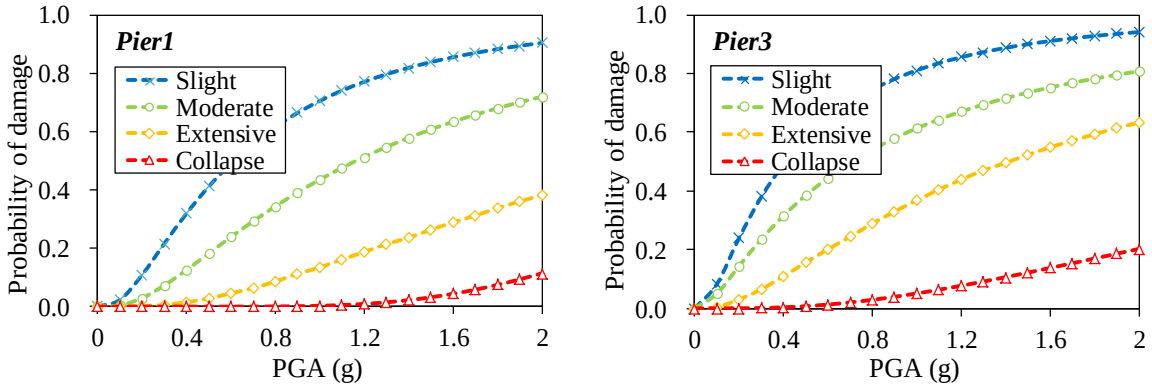

Figure 11. Fragility curves of the piers P1 & P3 for the base-isolated bridge

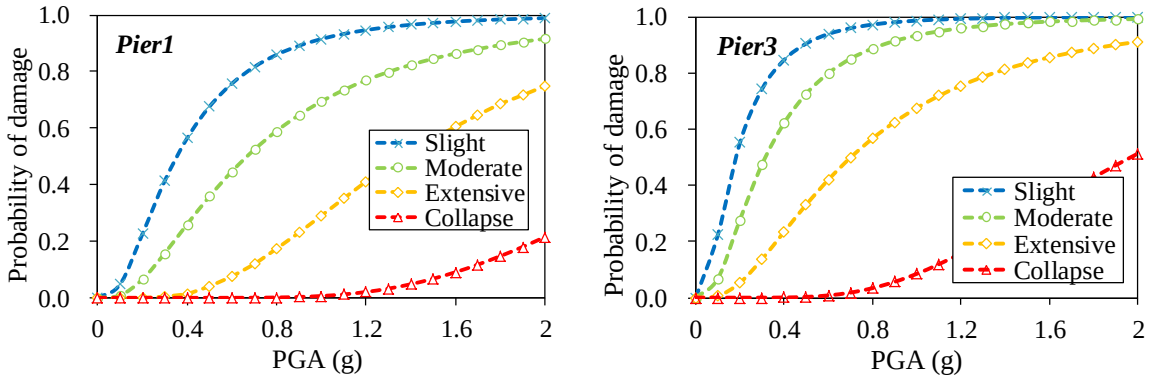

Figure 12. Fragility curves of the piers P1 & P3 for the non-isolated bridge

Figs 13 and 14 show a comparison of fragility curves of bridge piers applying worldwide earthquakes and ground motions in Korea for base-isolated and non-isolated bridges, respectively. Here, the "W" and "K" letters are abbreviated for Worldwide and Korean motions, respectively. It can be seen that at the same PGA level the bridges subjected to ground motion records in Korea are less vulnerable than imposed worldwide ground motions. This is attributed to the reason that the Korean response spectra at the fundamental period of structures are significantly smaller than those of the worldwide response spectra. In other words, the Korean motions are containing the high-frequency characteristics, while the fundamental frequency of structures is fallen in a small range. Consequently, the seismic responses of

the piers during Korean motions are diminutive than those of under the global earthquakes. The high-frequency features of Korean ground motions can be referred in the literature [20].

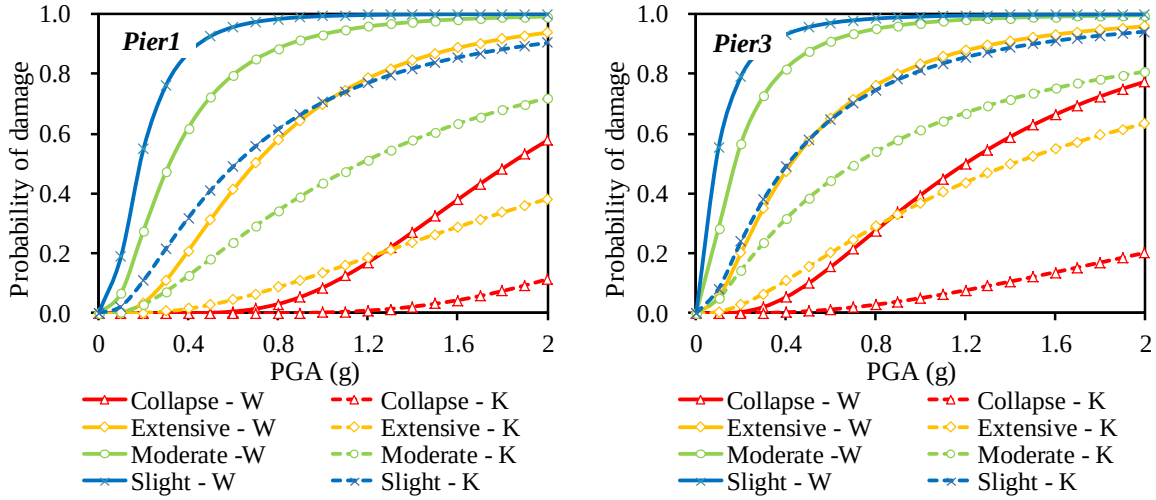

Figure 13. Comparison of fragility curves of the piers P1 & P3 for the base-isolated bridge

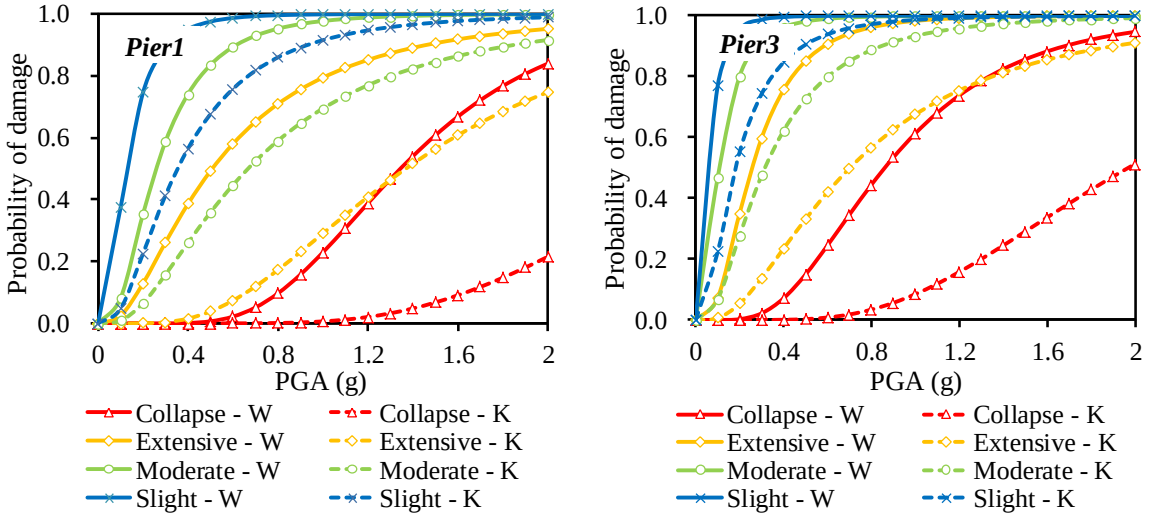

Figure 14. Comparison of fragility curves of the piers P1 & P3 for the non-isolated bridge

8. Conclusions

Seismic performance of a continuous steel box girder bridge with single-column RC piers was carried out using nonlinear time-history analyses. Two groups of ground motion records including worldwide earthquakes and Korean ground motions were considered in the fragility analyses. Based on the results, the main achievements are summarized as follows.

- The bridge piers are less vulnerable under Korean ground motions than that during worldwide earthquakes. The main cause is due to the high-frequency contents of the Korean ground motions.
- There is a significantly different seismic response between the piers at different positions of the bridge (e.g. at the ends and middle areas) in both cases with and without LRBs. Thus, the fragility analysis procedure should be conducted all the bridge piers for a sufficient assessment.
- The seismic damage probability of the non-isolated bridge is always higher than that of the base-isolated one.

A larger enough number of ground motions recorded in Korea is necessary in the fragility analysis to reduce the uncertainties of seismic loading. Additionally, the effect of soil-structure interaction phenomenon on the fragility assessment should be considered in the future study.

References

[1] Billah A H and Alam M S 2015 Seismic fragility assessment of highway bridges: a state-of-the-art review *Struct. and Infras. Eng.: Maint., Manag., Life-Cycle Des. and Perfor.* **11**(6):804-832
[2] Shinozuka M, Feng M Q, Kim H K and Kim S H 2000 Nonlinear static procedure for fragility curve development. *ASCE J. Eng. Mech* **126**:1287-1296
[3] Shinozuka M, Feng M Q, Lee J and Naganuma T 2000 Statistical analysis of fragility curves *ASCE J. Eng. Mech* **126**(12):1224-1231
[4] Karim K R and Yamazaki F 2003 A simplified method of constructing fragility curves for highway bridges *Earthq. Eng. Struct. Dyn* **32**:1603–1626
[5] Moschonas I F, Kapos A J, Panetsos P, Papadopoulos V, Makarios T and Thanopoulos P 2009 Seismic fragility curves for Greek bridges: Methodology and case studies *Bull. of Earthq. Eng.* **7**:439-468
[6] Choi E, DesRoches R and Nielson B G 2004 Seismic fragility of typical bridges in moderate seismic zones *Eng. Struct.* **26**:187–199
[7] Kibboua A, Naili M, Benouar D and Kehila F 2011 Analytical fragility curves for typical Algerian reinforced concrete bridge piers *Struct. Eng. and Mech.* **39**(3):411-415
[8] Tavares D H, Suescun J R, Paultre P and Padgett J E 2013 Seismic fragility of a highway bridge in Quebec *ASCE J. Bridg. Eng.* **18**(11): 1131-1139
[9] Lee S M, Kim T J and Kang S L 2007 Development of fragility curves for bridges in Korea *KSCE J. Civil Eng.* **11**(3):165-174
[10] Lee T H and Nguyen D D 2018 Seismic vulnerability assessment of a continuous steel box girder bridge considering influence of LRB properties *Sadhana* **43**, DOI: 10.1007/s12046-017-0774-x
[11] Abbasi M, Abedini M J, Zakeri B and Amiri G G 2016 Seismic vulnerability assessment of a Californian multi-frame curved concrete box girder viaduct using fragility curves *Struct. and Infras. Eng.: Maint., Manag., Life-Cycle Des. and Perfor.* **12**(12): 1585-1601
[12] Kim D K, Yi J H, Seo H Y and Chang C H 2008 Earthquake risk assessment of seismically isolated extradosed bridges with lead rubber bearings *Struct. Eng. and Mech.* **29**(6):689-707
[13] Ramanathan K, DesRoches R and Padgett J E 2010 Analytical fragility curves for multi span continuous steel girder bridges in moderate seismic zones *J. Transp. Research Board* **2202**:173-182
[14] Alam M S, Bhuiyan A R and Billah A M 2012 Seismic fragility assessment of SMA-bar restrained multi-span continuous highway bridge isolated with laminated rubber bearing in medium to strong seismic risk zones *Bull. of Earthq. Eng.* **10**:1885–1909.
[15] Mazzoni S, McKenna F, Scott M H and Fenves G L 2007 *OpenSees command language manual*. Pacific Earthquake Engineering Research Center (University of California, Berkeley, USA)
[16] Federal Highway Administration (FHWA) 2006 *Seismic Retrofitting Manual for Highway Structures: Part 1 – Bridges*, Publication No. FHWA-HRT-06-032 (Department of Transportation, McLean, Virginia, USA)
[17] Kent DC and Park R. Flexural members with confined concrete 1971 *ASCE J. Struct. Div.* **97**(7):1969-1990
[18] Menegotto M and Pinto PE 1973 Method of analysis for cyclically loaded reinforced concrete plane frames including changes in geometry and non-elastic behavior of elements under combined normal force and bending *Proc. IABSE Sym. of Resist. and Ult. Deform. of Struct. Acted on by Well-Defined Repeat. Loads* (Lisbon, Portugal) pp 15-22
[19] CSI 2011 *SAP2000 software*, ver15. Berkeley, California, USA
[20] Park H S, Nguyen D D, and Lee T H 2017 Effect of high-frequency ground motions on the response of NPP components: A state-of-the-art review *J. Korean Soc. Hazzard Mitig.* **17**(6) 285-294